Article

Grain Growth Behavior of Alumina in Zirconia-Toughened Alumina (ZTA) Ceramics During Pressureless Sintering

Yi Zhao [1], Jiang Deng [1], Wen Li [2], Jianhong Liu [2] and Wenjie Yuan [1,3,4,*]

[1] State Key Laboratory of Advanced Refractories, Wuhan University of Science and Technology, Wuhan 430081, China; zhaoyi2000816@163.com (Y.Z.); dj.1261188641@icloud.com (J.D.)

[2] Hubei Smile New Materials Co., Ltd., Huanggang 438400, China; lw@hbsmile.cn (W.L.); ljh@hbsmile.cn (J.L.)

[3] National-Provincial Joint Engineering Research Center of High Temperature Materials and Lining Technology, Wuhan University of Science and Technology, Wuhan 430081, China

[4] Joint International Research Laboratory of Refractories and Metallurgy, Wuhan University of Science and Technology, Wuhan 430081, China

* Correspondence: yuanwenjie@wust.edu.cn

Abstract: The primary grain size, sintering conditions, and admixtures have a significant impact on the grain growth of alumina ceramics. Three kinds of alumina powders with varying grain sizes and zirconia nanoparticles were selected and configured into five compositions of zirconia-toughened alumina (ZTA) ceramics. As-received granules were used to sinter bulk ceramics at temperatures of 1520 °C, 1600 °C, and 1680 °C for durations of 0.5–2 h, respectively. The average grain sizes of alumina in ZTA ceramics were studied as a function of the sintering temperature, time, and particle size of raw materials. The results demonstrated that the addition of nano alumina led to a slight reduction in the grain size of alumina and a more uniform grain size distribution. The incorporation of nano zirconia (15 wt.%) resulted in the concentration of zirconia among the alumina grains, effectively inhibiting grain growth and resulting in a significant reduction in the average grain size of alumina from 11.73 to 5.63 μm after sintering at 1600 °C for 1 h.

Keywords: ZTA ceramics; grain size; grain size distribution; sintering temperature; holding time

1. Introduction

Zirconia-toughened alumina (ZTA) ceramics are high-performance structural ceramic materials that have attracted considerable attention due to their excellent mechanical properties, thermal stability, and chemical inertness [1–3]. Alumina, as a matrix material, exhibits high strength, high hardness, and good wear resistance, while the addition of zirconia significantly enhances the toughness and crack resistance of materials [4–7]. This composite ceramic combines the rigidity of alumina with the toughness of zirconia and thus shows promise for use in a range of applications [8]. In order to alter the microstructure and achieve the desired properties of ceramics, the second phase is often incorporated in different ways. Better mechanical properties and uniform distribution of phases can be obtained for ZTA ceramics prepared by various aqueous colloidal processing routes with high cost and complexity [9]. A denser compact after the pressing of ZTA granules produced through the spray granulation process was expected to achieve a higher sintered density. It was demonstrated that ZTA ceramics with low ZrO_2 content (10 vol.%) exhibited better crack resistance [10]. The quality of ZTA ceramics depended on not only the particle size, shape, and composition of granules but also the grain size of the phases.

The primary grain size has a considerable impact on the properties of alumina ceramics following the sintering process [11]. It has been demonstrated that sintered ceramics exhibit enhanced densities and mechanical strength when the original grain size of raw materials is reduced [12]. Due to the fact that fine grains are more susceptible to diffusion and bonding during the sintering process, the formation of pores and defects is inhibited. Additionally, fine-grained alumina ceramics present better light transmission and wear resistance [13].

Furthermore, the addition of a specific quantity of zirconia has been demonstrated to effectively inhibit grain boundary migration and grain growth, thereby achieving the objective of grain refinement and enhancing the mechanical properties of materials [14]. In a study conducted by Basha and Sarkar, submicron alumina (200 nm) was employed, with 5 wt.% nano zirconia, and subsequently sintered at temperatures between 1400 °C and 1600 °C [15]. The results demonstrated that the fracture toughness and hardness of the ZTA ceramics exhibited an increase of 21% and 5%, respectively, and exhibited enhanced compressive and tensile strengths.

The sintering temperature represents a pivotal parameter in the preparation of alumina ceramics, with the selected temperature directly influencing the degree of densification and the microstructure of the ceramics [16]. Fan et al. prepared six sets of ZTA ceramic samples at temperatures ranging from 1100 to 1450 °C [17]. The findings indicated that the densification and mechanical properties of the samples increased with rising temperature, with the highest fracture toughness attained at 1450 °C. Nevertheless, excessively high sintering temperatures can result in unfavorable outcomes such as closed pores within the grains and abnormal grain growth, which reduces the densities and mechanical properties of ceramics [18].

Secondly, the duration of the holding period is also a significant factor influencing the sintering effect of alumina ceramics. An appropriate holding time is conducive to the full diffusion and combination of ceramic particles, thereby facilitating the formation of a dense microstructure [19]. However, a too-short holding time can result in insufficient densification of the material, which is susceptible to fracture and deformation. M. Golieskardi et al. investigated the impact of varying heat preservation times on zirconia ceramics, and the findings indicated that zirconia ceramics placed in heat preservation at 1450 °C for 2 h exhibited the most favorable overall performance and microstructure [20].

The properties of single-component (Al_2O_3) and multiphase (ZTA) ceramics can be improved by using granules made from submicron particles [21]. In comparison, the impact of micro-size alumina as a low-cost alternative starting material for ZTA granules is a noteworthy issue during the conventional pressureless sintering. In this work, three kinds of alumina powders were selected to prepare ZTA granules with 15 wt.% ZrO_2 and subjected to sintering under varying conditions (1520–1680 °C for 0.5–2 h) to evaluate the influence of alumina particle size, sintering parameters, and nano zirconia incorporation on the grain growth behavior of alumina. The results including the grain size distribution, grain growth index, and growth activation energy of alumina could serve as a reference for the selection of raw materials and the design of the sintering process.

2. Materials and Methods

Fine reactive alumina powders (AMA10, D_{50} = 0.8 μm, Hubei Smile New Material, Huanggang, China), calcined alumina powders (AMA40, D_{50} = 1.8 μm, Hubei Smile New Material), nano alumina powders (AEROXIDE Alu C, Evonik Resource Efficiency GmbH, Marl, Germany), yttrium oxide-stabilized zirconia (YSZ) (OZ-3Y-5, Guangdong Oriental Zirconium Co., Ltd., Shantou, China) were selected as raw materials. All raw materials and sintering aids were mixed according to the composition shown in Table 1, the corundum balls were used as the medium, and the ball mill was used to grind them with the SY-3

wet ball mill for 1 h. The homogeneously mixed slurry was transported by a peristaltic pump at the rate of 35 mL/min to the spray pelletizing tower for spray pelleting, and the temperature of the inlet air in the spray pelletizing tower was 240 °C and that of the outlet air was 140 °C.

Table 1. Composition of granules.

Recipe	Reactive Alumina (wt.%)	Calcined Alumina (wt.%)	YSZ (wt.%)	Nano Alumina (wt.%)
A	100	0	0	0
B	99	0	0	1
C	85	0	15	0
D	68	17	15	0
E	84	0	15	1

ZTA granules were loaded into a steel mold and subjected to dry pressing at a pressure of 80 MPa. The sintering process was carried out in a high-temperature furnace at elevated temperatures, as listed in Table 2. According to previous research reports, ZTA ceramics with 15 wt.% ZrO_2 presented the best mechanical properties [10,22]. Therefore, Combination E was selected for sintering at different temperatures and holding times.

Table 2. Sintering temperature and holding time of the samples.

Sample	Raw Material Formula	Sintering Temperature (°C)	Holding Time (h)
A	A	1600	1
B	B	1600	1
C	C	1600	1
D	D	1600	1
E1	E	1520	1
E2	E	1680	1
E3	E	1600	0.5
E4	E	1600	1
E5	E	1600	2

An SEM (JSM-6610, JEOL, Tokyo, Japan) was used to observe the microscopic morphology of the sintered samples. The particle size distribution of the granulated powders was measured using a vibrating screen. The phase compositions of the samples were analyzed using an X-ray diffractometer (X'pert Pro MPD, PANalytical, Almelo, The Netherlands). The grain size of the sintered samples was counted using ImageJ software, v1.54g version. The fracture toughness of the samples was determined by the indentation method. The density of the samples was measured using the Archimedean drainage method.

3. Results and Discussion

3.1. Particle Size Distribution of ZTA Granules

The particle size distributions of ZTA granules with different compositions are illustrated in Figure 1. Despite the differences in composition, the majority of powder sizes were in the range between 45 and 75 μm. Additionally, the particle sizes of granules exhibited a bimodal distribution, with over 90% of the sizes being less than 120 μm.
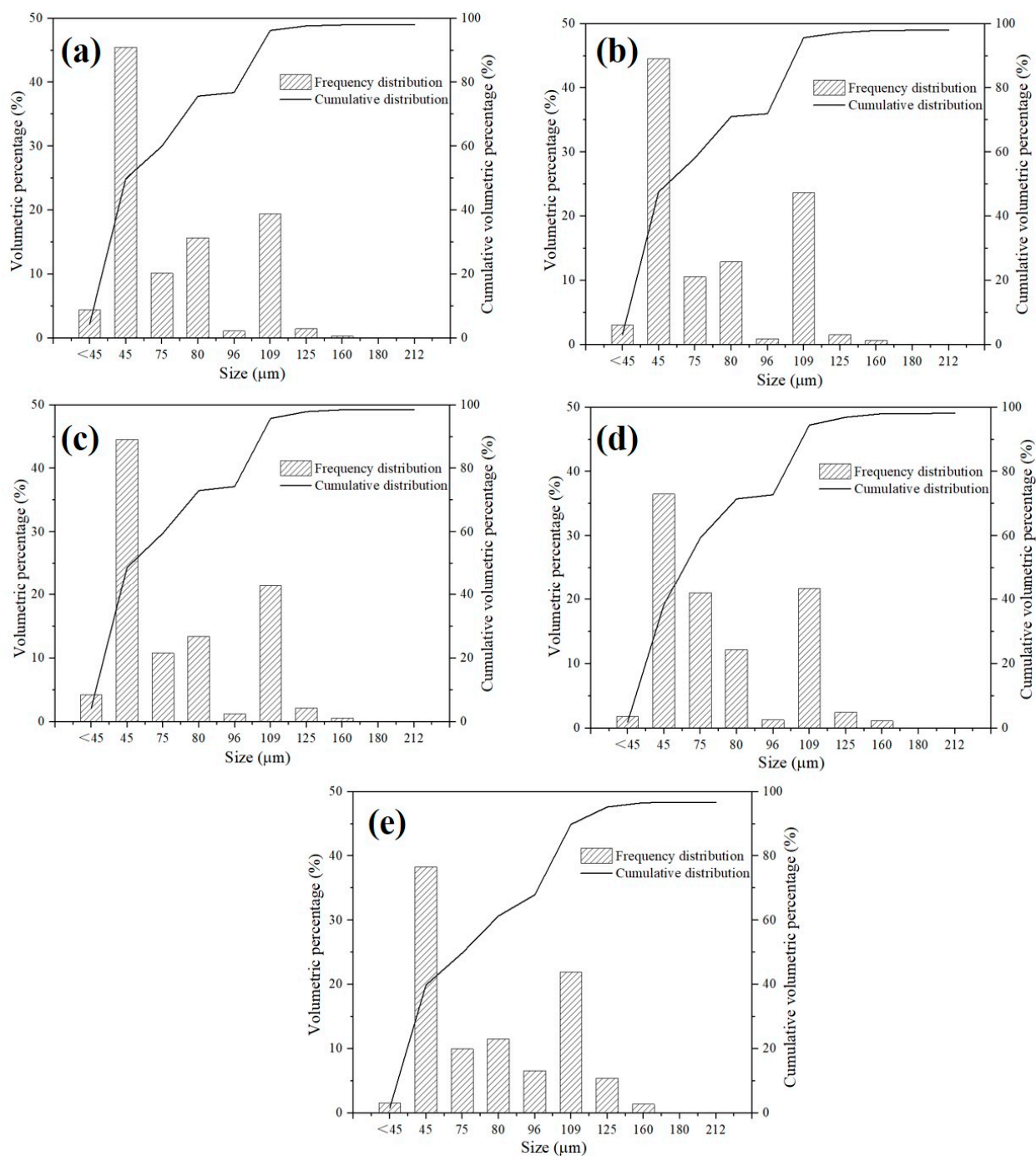
Figure 1. Frequency distribution (left Y-axis) and cumulative distribution (right Y-axis) of particle size of different compositions of granulated powder: (**a**) composition A; (**b**) composition B; (**c**) composition C; (**d**) composition D; and (**e**) composition E.

Table 3 presents the particle size data of the granulated powders. The D_{50} value ranged from 75 to 80 μm, while the D_{90}/D_{10} values were all approximately 2.40. Span described as the concentration of particle size distribution can be calculated by the formula presented in Equation (1). A smaller span value indicates a more uniform particle size distribution and a higher degree of size homogeneity. As can be observed from the data presented in Table 3, all of the granulated powders exhibit a satisfactory degree of particle size concentration, with values falling between 0.9 and 1. Composition **D** displays the most optimal concentration, which can be attributed to the presence of a defined particle grada-

tion, thereby resulting in the most favorable slurry flowability. The enhanced flowability exerts a beneficial influence on the homogeneity of the granulated powders.

$$Span = \frac{D_{90} - D_{10}}{D_{50}} \tag{1}$$

Table 3. Particle size and span of granulated powders.

Recipe	D_{10} (µm)	D_{50} (µm)	D_{90} (µm)	D_{90}/D_{10}	Span
A	48.7	75.1	119.9	2.46	0.95
B	48.9	75.6	120.7	2.47	0.95
C	49.7	76.1	121.2	2.44	0.94
D	51.7	77.8	121.7	2.35	0.90
E	51.6	80.3	126.2	2.45	0.93

3.2. Microstructure and Densities of Sintered ZTA Ceramics

The densities and shrinkage of the sintered samples were measured, and the average grain sizes of alumina were determined, as illustrated in Table 4. The sintered sample **A** made from reactive alumina (AMA10) exhibited the highest degree of densification (95.21%), yet its average grain size of alumina was the largest. The lowest sintering temperature resulted in the smallest grain size and the lowest densification for sample **E1**.

Table 4. Shrinkage, relative density of samples, and average grain size of alumina.

Sample Number	Shrinkage (%)	Relative Density (%)	Average Grain Size (µm)	Standard Deviation of Grain Size (µm)
A	18.24	95.21	11.73	0.31
B	18.78	94.61	10.85	0.30
C	17.52	94.33	8.25	0.23
D	16.86	95.13	5.47	0.11
E1	17.94	93.17	4.54	0.23
E2	18.64	94.11	8.26	0.19
E3	18.67	94.90	5.55	0.13
E4	18.51	94.98	5.63	0.23
E5	18.19	94.79	5.96	0.14

Figure 2 depicts the microstructure of samples **A**–**D**. The images illustrate that the grain size of sample **A** was substantial, which exhibited a non-uniform distribution, accompanied by conspicuous abnormal grain growth and the presence of pronounced pores on the grains. In comparison to sample **A**, the anomalous growth phenomenon was markedly diminished as a consequence of the incorporation of 1 wt.% of alumina nanoparticles into sample **B**. Upon examination of the coarsening rate β (defined as the post-firing grain size/original grain size) of samples **A** and **B**, it was observed that the value of β underwent a mere reduction from 14.67 to 13.56, and the grain coarsening phenomenon remained unimproved. Samples **C** and **D** exhibited reductions in grain size of 30% and 53%, respectively, compared to other samples, attributed to the incorporation of zirconia. No abnormally grown grains were found in the micrographs. The statistical results (seen in Figure 3) show that the addition of zirconia nanoparticles had a significant effect on inhibiting the growth of alumina grains.
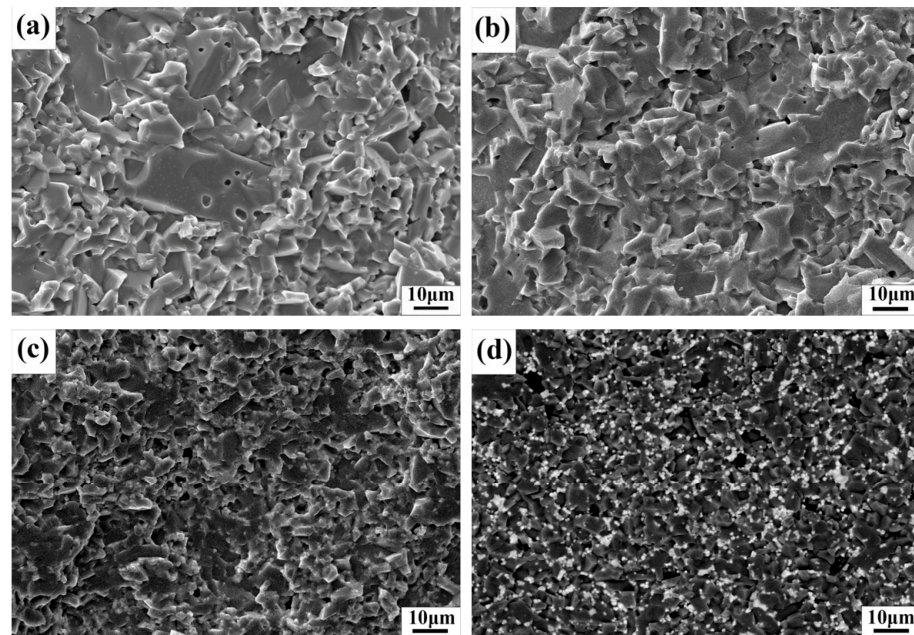
Figure 2. Microstructures of samples A–D: (**a**) sample A; (**b**) sample B; (**c**) sample C; and (**d**) sample D.
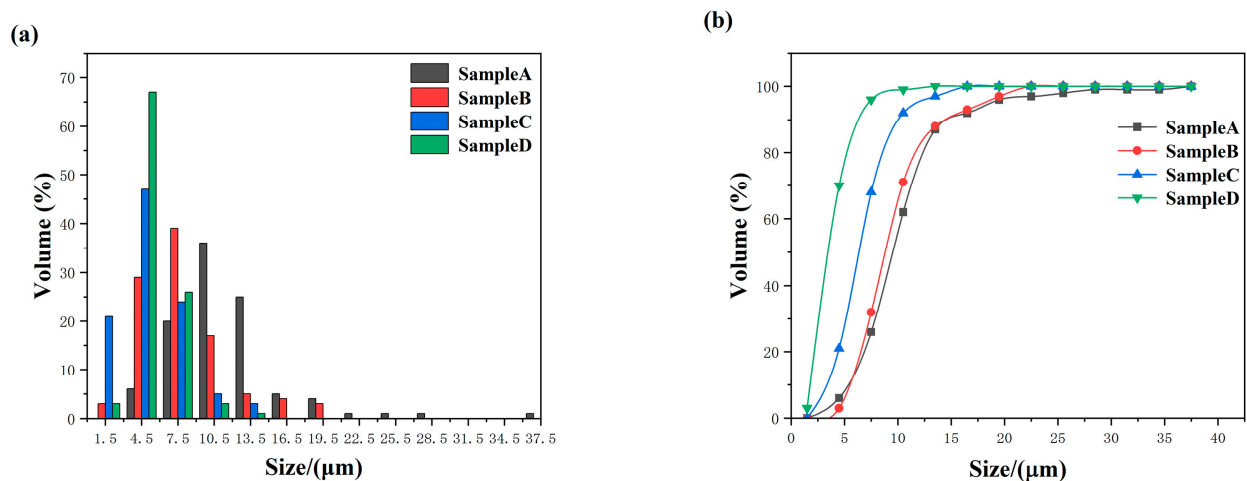
Figure 3. Grain size distribution of alumina in samples A–D: (**a**) Frequency distribution and (**b**) Cumulative distribution.

Figure 2c,d illustrate the backscattered electron images of samples **C** and **D**, wherein the white grains are identified as zirconia and the black matrix is designated as alumina. The zirconia grains were situated between the alumina grains, which were primarily distributed at the triple junction of the alumina grain boundaries, with a minor proportion located within the alumina grains. The fast-growing grains were constrained by the slow-growing grains due to the constraints between grains, which resulted in the slow-growing grains being dissolved or dragged by the grain boundaries during the growth process, thus aggregating at the triple junctions [23]. It was evidenced that the growth of zirconia grains aggregated at the triple junctions of the alumina grains occurred, yet they did not merge to form a single and large grain. As indicated by the phase diagrams Al_2O_3-ZrO_2, zirconia is almost insoluble in alumina, thereby precluding the formation of a solid solution [24]. As illustrated in Figure 2d, the alumina grains are observed to be smaller in size at the elevated zirconia concentration, while at the reduced zirconia concentration, some of the alumina grains undergo growth and engulf the surrounding zirconia. The low zirconia content in this region results in insufficient zirconia distribution in the triple

junction between the alumina grains. Consequently, the growth of alumina grains is not significantly impeded by the second phase in such circumstances. The alumina expands and engulfs the surrounding zirconia grains, forming intragranular zirconia [25,26]. The accumulation of zirconia particles at the narrowest points of alumina grain growth and the inhibitory effect of these particles on alumina grain growth led to an increase in porosity, which hindered the densification process and made the ZTA ceramics less dense than the pure alumina ceramics.

X-ray diffraction (XRD) patterns of the granulated powders and the sintered ceramic samples are shown in Figure 4. The diffraction pattern indicated that approximately half of the zirconia in the raw material was m-ZrO_2 (m-tetrahedral zirconia), while the remaining half was t-ZrO_2. Additionally, alumina was predominantly α-Al_2O_3 (corundum). The diffraction pattern of sintered samples demonstrated that m-ZrO_2 almost disappeared, with only the t-ZrO_2 remaining, which can be attributed to the presence of CaO and Ca^{2+} in the fluxes added during the sintering process. The ionic radius of Ca^{2+} was similar to that of Zr^{4+}, and thus, Ca^{2+} can replace Zr^{4+} in ZrO_2 to form a substitutional solid solution, which prevented the phase transformation of zirconia.
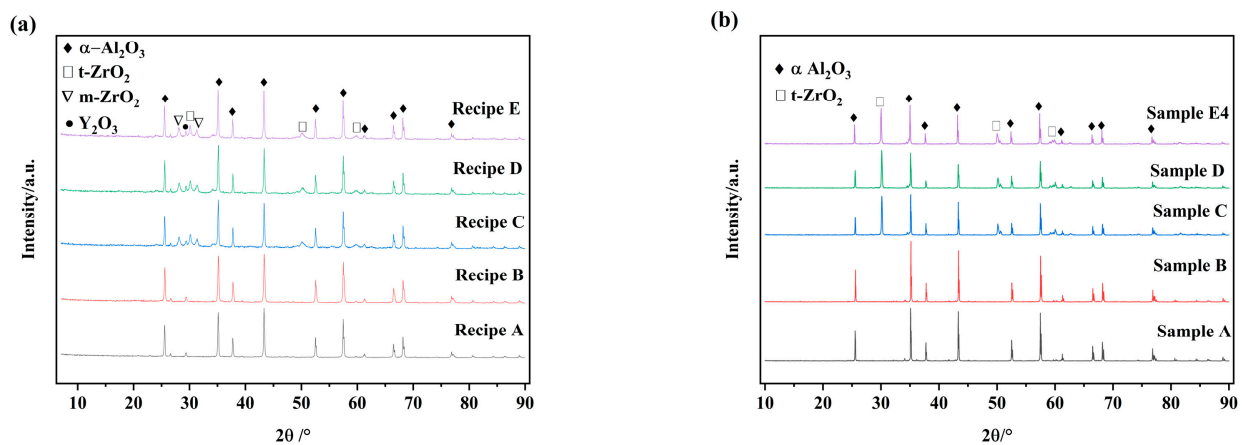
Figure 4. XRD patterns of granulated powder and post-fired samples. (**a**) Granulated powders; (**b**) The sintered samples.

The fracture toughness of sample **C** with zirconia nanoparticles was calculated by Vickers hardness indentation to be 6.99 MPa·m$^{1/2}$, which was 186.5% higher than that of sample **A** (2.44 MPa·m$^{1/2}$). The mismatch of the thermal expansion coefficient between zirconia and alumina, coupled with the latter's high modulus of elasticity, resulted in tetragonal zirconia particles undergoing compressive stress following sintering and cooling. When subjected to external forces, zirconia undergoes a stress-induced phase transition. During this process, the volume expansion energy couple absorbs part of the energy while generating microcracks, which serve to disperse the main cracks and alter the direction of crack expansion. Thus, an increase in the toughness of ZTA was presented. The dissimilar lattice constants between intracrystalline zirconia particles and alumina led to the generation of an elastic stress field at the interfaces, which also effectively inhibited the formation of dislocations and deflected the propagation of cracks. Wenya Du et al. demonstrated that the toughening effect of zirconia in the intracrystalline type was more pronounced [27].

The ratio of alumina powders AMA10 and AMA40 in sample **D** was four, which resulted in the formation of a specific particle gradation and yielded a sample with elevated densities and finer grains. The growth of alumina with small primitive grains commenced at lower temperatures. During the intermediate and final stages of sintering, the grain boundaries extended to the surface of the coarse particles, which acted as an obstacle to grain growth. This resulted in the formation of more homogeneous and finer grains [28].

Samples **E1**–**E5** were sintered under varying conditions for composition **E**, and the microstructural photographs are presented in Figure 5. Samples **E1**, **E2**, and **E4** exhibited only minor differences in microstructures, despite the significant variation in sintering temperature. The driving force for sintering increased as the sintering temperature was increased from 1520 °C to 1600 °C. The mean grain size increased from 4.54 to 5.63 µm, representing 24% growth. This suggests that grain development is susceptible to fluctuations in temperature. Figure 6 illustrates the grain size distribution of the samples. The frequency distribution graph indicates that the peak of the frequency of grain size concentration shifts to the right as the temperature increases.
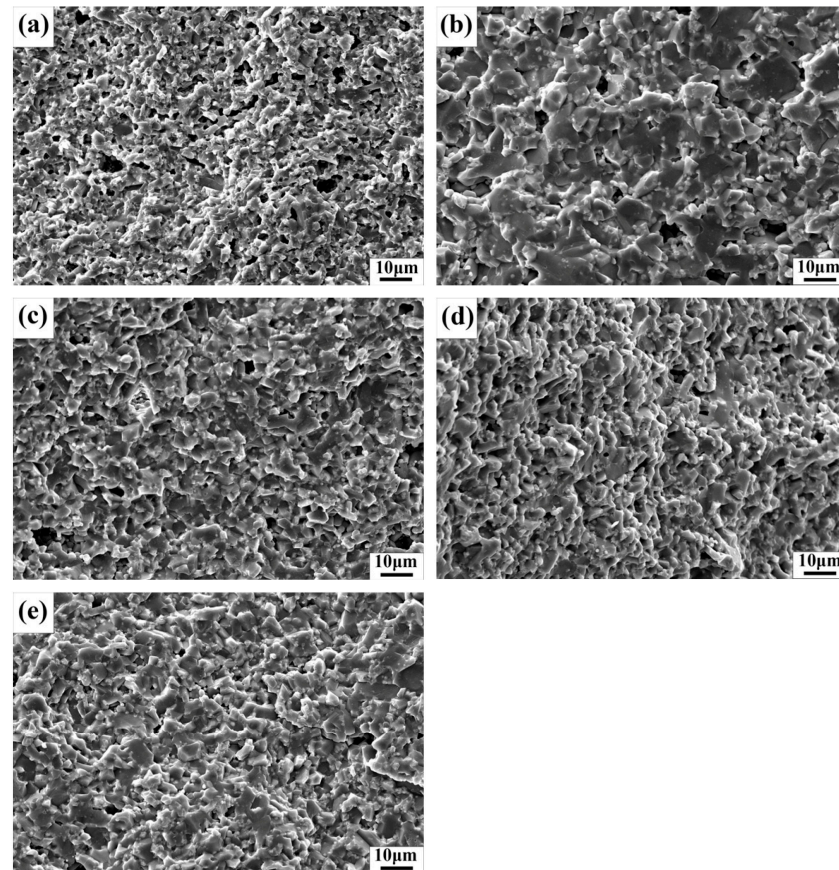
Figure 5. Microstructure of samples E1–E5: (**a**) sample E1; (**b**) sample E2; (**c**) sample E3; (**d**) sample E4; and (**e**) sample E5.
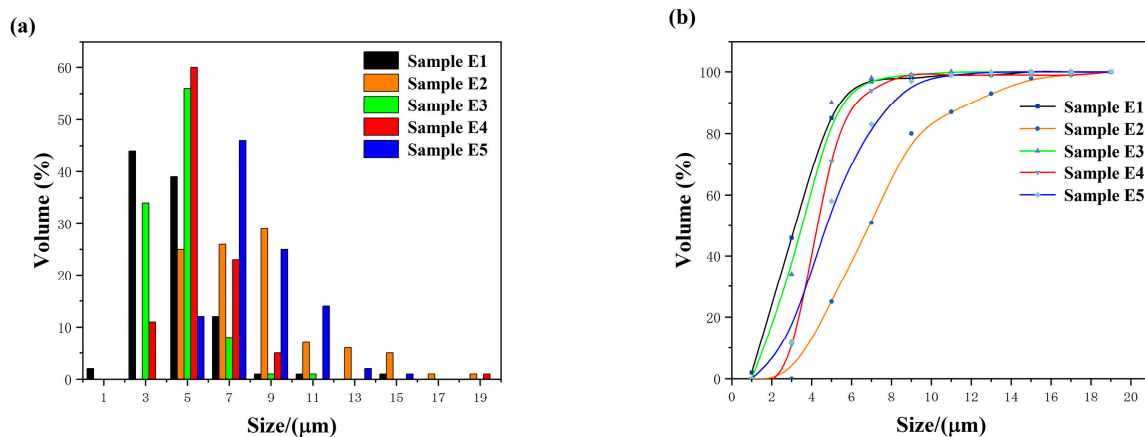
Figure 6. Grain size distribution of alumina in samples E1–E5: (**a**) frequency distribution and (**b**) cumulative distribution.

Upon elevating the sintering temperature to 1680 °C, a notable coarsening of the grains in the samples was observed, accompanied by an expansion in the range of grain size distributions. This phenomenon can be attributed to the overgrowth of grains resulting from the application of a high sintering temperature [29]. The mean grain size increased to 8.26 μm, representing 46.7% amplification relative to the grain size at 1600 °C. The growth rate of alumina grains at 1520, 1600, and 1680 °C was not linear with increasing temperature. In comparison with sample **B**, sample **E2** incorporated 15 wt.% of zirconia nanoparticles, and the presence of zirconia particles significantly reduced the migration rate at the alumina grain boundaries. Despite the higher sintering temperature of sample **E2** relative to sample **B**, the grain size was substantially reduced, and the β-value decreased from 13.56 to 10.33, thereby suppressing grain coarsening. This finding indicated that zirconia particles exerted a more pronounced effect on hindering grain boundary migration and refining grains in relation to temperature.

Samples **E3** to **E5** were sintered at 1600 °C for 0.5 h, 1 h, and 2 h, respectively, for formulation **E**. As demonstrated in Table 4, the change in density and grain size of the samples as a function of holding time was negligible. As demonstrated in Figure 6, samples **E3** to **E5** exhibited a satisfactory concentration and uniformity of grain size. It was generally accepted that prolonging the holding time can effectively promote grain growth, thereby enhancing the removal of porosity and facilitating the densification of ceramics [30]. As illustrated in Figure 5, microstructure photographs indicated a tendency for a gradual increase in grain size with increasing holding time, despite the densities of the samples remaining unchanged. Even if the holding time was extended up to 34 h, the densification of ZTA ceramics was not greatly changed [31].

The present results demonstrated that the growth of alumina grains depended on multiple factors. The addition of 15 wt.% ZrO_2 nanoparticles exhibited the most significant effect on grain growth, followed by the sintering temperature. The holding time during the experiment had a negligible impact on grain size. Regarding the influence of a dispersed second phase on grain growth, it has been suggested that the grain-growth inhibition derived by zirconia should be categorized as Zener's pinning effect [32]. According to Zener's model, a pinning effect is anticipated to arise when the ratio of the average grain size of alumina (D) to the radius of zirconia particles (r) is proportional to the inverse of the volume percentage of the second phase (f), specifically expressed as $D/r \propto 1/f$ [33,34]. Despite this relationship proved to be invalid due to the aggregation of particles when the volume fraction of zirconia exceeded 10 vol.% [35], the ratio of D/r could still be compared with each other. Moreover, the value depended on the uniformity of the dispersion of zirconia particles within alumina as well as the particle size of raw materials. The ZTA ceramics with the addition of 10 vol.% zirconia containing 12 mol.% CeO_2 corresponded to D/r of 4.6 [23]. In the present work, the volume fraction of zirconia was approximately 11 vol.%, and the calculated ratios of D/r ranged from 7.3 to 8.0, which was close to the values of alumina ceramics with less zirconia [36]. Thus, Zener's pinning effect was partially diminished due to the clustering of zirconia particles.

3.3. Grain Growth Kinetics

For ZTA ceramics, the grain growth during sintering is calculated using Equation (2) [37,38]:

$$G^n = K_0 t \exp\left(-\frac{Q}{RT}\right) \tag{2}$$

where G is the grain size (μm), n is the grain growth index, K_0 is a constant, t is the holding time (h), Q is the activation energy for grain growth (kJ/mol), R is a constant (8.31 J/(mol·K)), and T is the temperature (K).

Simultaneously taking the logarithms on both sides yields a function of the logarithm of time, as follows:

$$nlnG = \left(lnK_0 - 0.434\frac{Q}{RT} \right) + lnt \tag{3}$$

To obtain the value of the sintering activation energy, Q, the above equation can be transformed as follows:

$$ln\frac{G^n}{t} = -\frac{0.43Q}{R} * \frac{1}{T} + lnk_0 \tag{4}$$

As illustrated in Figure 7, the parameters of grain growth index and grain growth activation energy are demonstrated. The data for composition **E**, held at 1600 °C for varying periods, were incorporated and fitted linearly to obtain $n = 4.57$, which was indicative of boundary diffusion-controlled grain growth [23,39]. The n value signified the mechanism of the inhibition of grain growth in this system, with a larger n value indicating stronger inhibition of grain growth and slower alumina grain growth. By fitting the $ln\frac{G^n}{t} - \frac{1}{T}$ function, the slope K is obtained ($K = \frac{0.43Q}{R}$), which in turn gives an activation energy for grain growth of 483.1 kJ/mol. This indicates that the addition of 15 wt.% zirconia has a pronounced inhibitory effect on grain growth.

(a)　　　　　　　　　　　　　　　　　　　　　　　　　　**(b)**
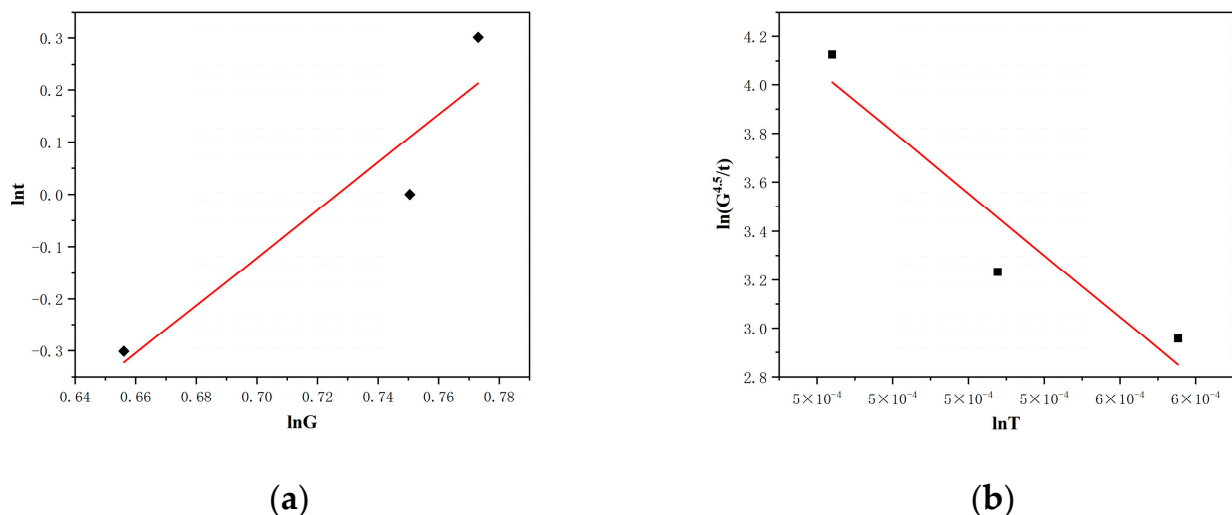
Figure 7. Fitting of grain growth index n (**a**), and growth activation energy Q (**b**).

In the study conducted by W.Y. Du, the incorporation of 7 vol.% zirconia into alumina led to a growth index n of 3.97 and activation energy for alumina grain growth of 429.19 kJ/mol [40]. Lange and Hirlinger posit that at least 7 vol.% of zirconia must be added to alumina and dispersed uniformly in the intercalation of alumina grains to completely inhibit the anomalous growth of alumina grains [41]. The values of n and the activation energy for grain growth with 11 vol.% of zirconia addition observed in the present study were greater than those above.

4. Conclusions

A total of five ZTA compositions were subjected to testing, with the granulated powders being prepared through the spray granulation method. Following dry press molding, the powder was held at temperatures of 1520 °C, 1600 °C, and 1680 °C for periods of 0.5 h, 1 h, and 2 h, respectively.

(1) The sintered alumina only comprising reactive alumina powders at 1600 °C for 1 h exhibited the highest degree of densification, although the phenomenon of abnormal grain growth was pronounced. The incorporation of nano alumina was demonstrated to effectively mitigate the issue of non-uniform grain size. Furthermore, the particle gradation

of the original grains can achieve high densities and finer grains. The addition of 15 wt.% YSZ suppressed the growth of alumina grains, consequently promoting the development of finer grain structures.

(2) The majority of zirconia grains were situated between the corners of alumina grains, effectively inhibiting grain growth. A limited quantity of zirconia trapped within alumina grains remained small, while alumina grains expanded and engulfed smaller grains in their vicinity.

(3) The sintering temperature had a significant impact on the densification process. ZTA ceramics containing 15% YSZ and 1% nano alumina achieved a relative density of 93.17%, 94.98%, and 94.11% at 1520 °C, 1600 °C, and 1680 °C, respectively, with a one-hour holding time. While the duration of the holding period in this study has a negligible impact on the degree of densification, an increase in the holding time resulted in a slight growth in grain size.

(4) The grain growth index and growth activation energy of alumina were calculated as 4.57 and 483.1 kJ/mol, respectively. The addition of zirconia markedly inhibited the growth of alumina grains, resulting in the formation of smaller grains.

References

1. Zhu, L.; Xu, Y.D.; Liu, S.W.; Chen, H.H.; Tao, J.; Tong, X.; Li, Y.; Huang, S.; Lin, J.; Wen, C.; et al. Microstructure, mechanical properties, friction and wear performance, and cytotoxicity of additively manufactured zirconia-toughened alumina for dental applications. *Compos. Part B Eng.* **2023**, *250*, 110459. [CrossRef]

2. Mangalaraja, R.V.; Chandrasekhar, B.K.; Manohar, P. Effect of ceria on the physical, mechanical and thermal properties of yttria stabilized zirconia toughened alumina. *Mater. Sci. Eng. A* **2003**, *343*, 71–75. [CrossRef]

3. Kyomoto, M.; Shoyama, Y.; Saiga, K.; Moro, T.; Ishihara, K. Reducing fretting-initiated crevice corrosion in hip simulator tests using a zirconia-toughened alumina femoral head. *J. Biomed. Mater. Res. Part B* **2018**, *106*, 2815–2826. [CrossRef] [PubMed]

4. Li, K.L.; Li, W.; Yi, Y.L. Interface characteristics and wear resistance of Ni-B_4C plated ZTA reinforced high chromium cast iron composite. *China Foundry* **2023**, *20*, 253–262. [CrossRef]

5. Ding, Z.Z.; Zreiqat, H.; Mirkhalaf, M. Rationally-designed self-shaped ceramics through heterogeneous green body compositions. *Mater. Horiz.* **2022**, *9*, 2762–2772. [CrossRef] [PubMed]

6. Wade-Zhu, Y.; Wade-Zhu, J.; Wu, H.; Binner, J.; Vaidhyanathan, B. The ballistic impact performance of nanocrystalline zirconia-toughened alumina (nZTA) and alumina ceramics. *J. Eur. Ceram. Soc.* **2021**, *41*, 1427–1437. [CrossRef]

7. Chen, J.Q.; Wang, W.L.; Sun, X.N.; Sun, G.X.; Liang, Y.J. Microstructure and mechanical properties of zirconia toughened nacre-like alumina ceramics. *Mater. Sci. Eng. A* **2022**, *855*, 143908. [CrossRef]

8. Wang, Y.; Jin, Z.; Feng, G.; Cao, J.; Zhang, H.; Deng, D. Characterization of ZTA composite ceramic/Ti6Al4V alloy joints brazed by AgCu filler alloy reinforced with one-dimensional $Al_{18}B_4O_{33}$ single crystal. *Crystals* **2022**, *12*, 933. [CrossRef]

9. Olhero, S.M.; Ganesh, I.; Torres, P.M.C.; Alves, F.J.; Ferreira, J.M.F. Aqueous colloidal processing of ZTA composites. *J. Am. Ceram. Soc.* **2010**, *92*, 9–16. [CrossRef]

10. Wang, X.; Tian, J.; Yu, X.; Shan, Y.; Liu, Z.; Yin, Y. Effect of microstructure on the fracture behavior of micro–nano ZTA composite. *Mater. Chem. Phys.* **2008**, *112*, 213–217. [CrossRef]

11. Li, J.; Cai, Q.; Luo, G.; Zhong, X.; Shen, Q.; Tu, R.; Guo, X.; Ding, R. Zirconia toughened alumina ceramics via forming intragranular structure. *Materials* **2024**, *17*, 1309. [CrossRef] [PubMed]

12. Niu, B.; Cai, D.L.; Yang, Z.H.; Duan, X.M.; Sun, Y.; Li, H.; Duan, W.; Jia, D.; Zhou, Y. Anisotropies in structure and properties of hot-press sintered h-BN-MAS composite ceramics: Effects of raw h-BN particle size. *J. Eur. Ceram. Soc.* **2019**, *39*, 539–546. [CrossRef]

13. O, Y.T.; Koo, J.B.; Hong, K.J.; Park, J.S.; Shin, D.C. Effect of grain size on transmittance and mechanical strength of sintered alumina. *Mater. Sci. Eng. A* **2004**, *374*, 191–195. [CrossRef]

14. Basha, S.A.; Sarkar, D. Grain growth suppression of ZTA by multi-step sintering. *Mater. Today Proc.* **2020**, *26*, 1226–1230. [CrossRef]

15. Yang, X.; Guo, J.; Xie, H.; Li, Y.; Yang, X. Preparation of ZTA composite ceramics derived from sol-gel method by DIW printing. *Int. J. Appl. Ceram. Technol.* **2024**, *21*, 3851–3862. [CrossRef]

16. Fan, J.Y.; Lin, T.T.; Hu, F.X.; Yu, Y.; Ibrahim, M.; Zheng, R.; Huang, S.; Ma, J. Effect of sintering temperature on microstructure and mechanical properties of zirconia-toughened alumina machinable dental ceramics. *Ceram. Int.* **2017**, *43*, 3647–3653. [CrossRef]

17. Chen, Y.; Fan, B.; Shao, G.; Zhang, R. Preparation of large size ZTA ceramics with eccentric circle shape by microwave sintering. *J. Adv. Ceram.* **2016**, *5*, 291–297. [CrossRef]

18. Chen, Y.A.; Tan, J.L.; Sun, J.X.; Guo, H.; Bai, J.; Zhou, P.; Zhang, D.; Liu, G. Effect of sintering temperature on the microstructures and mechanical properties of ZrO_2 ceramics fabricated by additive manufacturing. *Ceram. Int.* **2024**, *50*, 11392–11399. [CrossRef]

19. Chen, I.W.; Wang, X.H. Sintering dense nanocrystalline ceramics without final-stage grain growth. *Nature* **2000**, *404*, 168–171. [CrossRef]

20. Golieskardi, M.; Satgunam, M.; Ragurajan, D. Effect of holding time on the mechanical properties and microstructural evaluation of 3Y-TZP ceramics. *J. Aust. Ceram. Soc.* **2017**, *53*, 1001–1006. [CrossRef]

21. Tahir, A.; Rasche, S.; Könke, C. Discrete element model development of ZTA ceramic granular powder using micro computed tomography. *Adv. Powder Technol.* **2018**, *29*, 3471–3482. [CrossRef]

22. Mullot, J.; Lecompte, J.P.; Montanaro, L.; Negro, A. Influence of powder drying route on the mechanical properties of alumina-zirconia composites. *J. Eur. Ceram. Soc.* **1993**, *11*, 309–313. [CrossRef]

23. Alexander, K.B.; Becher, P.F.; Waters, S.B.; Bleier, A. Grain growth kinetics in alumina-zirconia (CeZTA) composites. *J. Am. Ceram. Soc.* **1994**, *77*, 939–946. [CrossRef]

24. Zhao, H.L.; Shen, J.Y.; Lu, W.H. Study on the structural characteristics of phase diagram of Al_2O_3-ZrO_2-SiO_2 system. *J. Chin. Ceram. Soc.* **1991**, *3*, 280–288.

25. Pan, X.; Mayer, J.; Rühle, M.; Niihara, K. Silicon nitride based ceramic nanocomposites. *J. Am. Ceram. Soc.* **1996**, *79*, 585–590. [CrossRef]

26. Orlovská, M.; Húlek, L.; Bača, Ľ.; Kovár, V.; Tomanová, K.; Kitzmantel, M.; Janek, M.; Neubauer, E. Neubauer. Study of the alumina sintering process with a low zirconia content. *Ceram. Int.* **2022**, *48*, 2736–2743. [CrossRef]

27. Du, W.Y.; Ai, Y.; He, W.; Chen, W.; Liang, B.; Lv, C. Formation and control of "intragranular" ZrO_2 strengthened and toughened Al_2O_3 ceramics. *Ceram. Int.* **2020**, *46*, 8452–8461. [CrossRef]

28. Xing, Y.Y.; Wu, H.B.; Liu, X.J.; Huang, Z.R. Influence of particle-level pairing on solid-phase sintered silicon carbide ceramics. *J. Inorg. Mater.* **2018**, *33*, 1167–1172. (In Chinese) [CrossRef]

29. Lóh, N.J.; Simão, L.; Jiusti, J.; De Noni, A., Jr.; Montedo, O.R.K. Effect of temperature and holding time on the densification of alumina obtained by two-step sintering. *Ceram. Int.* **2017**, *43*, 8269–8275. [CrossRef]

30. Chen, X.; Lu, T.; Wei, N.; Hua, T.; Zeng, Q.; Wu, Y. Fabrication and microstructure development of Yb: YAG transparent ceramics from co-precipitated powders without additives. *J. Am. Ceram. Soc.* **2019**, *102*, 7154–7167. [CrossRef]

31. Witek, S.R.; Butler, E.P. Zirconia particle coarsening and the effects of zirconia additions on the mechanical properties of certain commercial aluminas. *J. Am. Ceram. Soc.* **1986**, *69*, 523–529. [CrossRef]

32. Smith, C.S. Grains, phases, and interfaces an interpretation of microstructure. *Metal. Technol.* **1948**, *175*, 15–51.

33. Hellman, P.; Hillert, M. On the effect of second-phase particles on grain growth. *Scand. J. Metall.* **1975**, *4*, 211–219.

34. Hillert, M. Inhibition of grain growth by second-phase particles. *Acta Metall.* **1988**, *36*, 3177–3181. [CrossRef]

35. Hassold, G.N.; Holm, E.A.; Srolovitz, D.J. Effects of particle size on inhibited grain growth. *Scripta Metal. Mater.* **1990**, *24*, 101–106. [CrossRef]

36. Okada, K.; Sakuma, T. The role of Zener's pinning effect on the grain growth in Al_2O_3-ZrO_2. *J. Ceram. Soc. Jpn.* **1992**, *100*, 382–386. [CrossRef]

37. Gonzalez, J.L.; Piumbini, C.K.; Scopel, W.L.; Deleprani, F.; Gomes, A.; Cunha, A. Pore structure dependence with the sintering time for dense ceramic bulk $YBa_2Cu_3O_y$. *Ceram. Int.* **2013**, *39*, 3001–3006. [CrossRef]

38. Cheng, M.; Liu, W.S.; Yao, S.W.; Wang, J.; Ma, Y.Z. Kinetics and mechanisms for the densification and grain growth of the α-alumina fibers isothermally sintered at elevated temperatures. *Ceram. Int.* **2022**, *48*, 21756–21762. [CrossRef]

39. Voytovych, R.; MacLaren, I.; Gülgün, M.A.; Cannon, R.M.; Rühle, M. The effect of yttrium on densification and grain growth in α-alumina. *Acta Mater.* **2002**, *50*, 3453–3463. [CrossRef]

40. Du, W.Y. Formation control and growth kinetics of "endocrystalline" ZrO_2/Al_2O_3 composite ceramics. Master's Thesis, Nanchang Hangkong University, Nanchang, China, 2020. (In Chinese)

41. Lange, F.F.; Hirlinger, M.M. Hindrance of grain growth in Al_2O_3 by ZrO_2 inclusions. *J. Am. Ceram. Soc.* **1984**, *67*, 164–168. [CrossRef]